

## Impairment of ATPase, adenine nucleotide translocator, and adenylate kinase causes mitochondrial energy deficit in human skin fibroblasts with chromosome 21 trisomy

Daniela VALENTI<sup>\*1</sup>, Apollonia TULLO<sup>†</sup>, Mariano Francesco CARATTOZZOLO<sup>†</sup>, Riccardo Sandro MERAFFINA<sup>\*</sup>, Paolo SCARTEZZINI<sup>‡</sup>, Ersilia MARRA<sup>\*</sup>, Rosa Anna VACCA<sup>\*1</sup>

<sup>\*</sup>Institute of Biomembranes and Bioenergetics, National Research Council (CNR), 70126 Bari, Italy.

<sup>†</sup>Institute for Biomedical Technologies, National Research Council (CNR), 70126 Bari, Italy.

<sup>‡</sup>Department of Gerontology and Motor Sciences, Galliera Hospitals, 16128 Genova, Italy.

<sup>1</sup>Correspondence may be addressed to either D. Valenti or R.A. Vacca (email: [d.valenti@biologia.uniba.it](mailto:d.valenti@biologia.uniba.it) or [r.vacca@ibbe.cnr.it](mailto:r.vacca@ibbe.cnr.it)).

**Short title:** Mitochondrial energy deficit in Down syndrome

### Synopsis

A central role for mitochondrial dysfunctions has been proposed in the pathogenesis of Down syndrome (DS), a multifactorial disorder caused by trisomy of human chromosome 21.

To explore whether and how abnormalities in mitochondrial energy metabolism are involved in DS pathogenesis, we investigated the catalytic properties, gene expression and protein levels of certain proteins involved in mitochondrial ATP synthesis such as ATPase, ADP/ATP translocator (ANT) and adenylate kinase (AK) in human skin fibroblasts from subjects with DS (DS-HSF) comparing them with euploid fibroblasts.

In DS-HSF, we found a strong impairment of mitochondrial ATP synthesis due to a reduction in the catalytic efficiency of each of the investigated proteins. This impairment occurred in spite of unchanged gene expression and an increase in ANT and AK protein content, whereas the amount of ATPase subunits was selectively reduced. Interestingly, exposure of DS-HSF to dibutyryl-cAMP, a permanent derivative of cAMP, stimulated ANT, AK and ATPase activities whereas H89, a specific PKA inhibitor, suppressed this cAMP-dependent activation, indicating an involvement of cAMP/PKA-mediated signalling pathway in ATPase, ANT and AK deficit. Consistently, DS-HSF showed decreased basal levels of cAMP and reduced PKA activity.

Despite the impairment of mitochondrial energy apparatus, no changes in cellular energy status but increased basal levels of L-lactate were found in DS-HSF which partially offset for mitochondrial energy deficit by increasing glycolysis and mitochondrial mass.

These results give new insight into the molecular basis for mitochondrial dysfunction in DS and might provide a molecular explanation for some clinical features of the syndrome.

**Keywords:** Down syndrome, mitochondria, ATPase, adenine nucleotide translocator, adenylate kinase, cAMP levels.

**Abbreviations:** AA, antimycin A; AK, adenylate kinase; ANT, adenine nucleotide translocator; Ap5A, diadenosine pentaphosphate; ASC, ascorbate; ATP-ds, ATP detecting system; CAT, carboxyatractyloside; Cox II, cytochrome *c* oxidase II; DS, Down syndrome; DS-HSF, human skin fibroblasts with trisomic karyotype; DS-HSF<sub>+DIG</sub>, digitonin-permeabilized human skin fibroblasts with trisomic karyotype; db-cAMP, dibutyryl-cAMP; FCCP, carbonylcyanide *p*-trifluoromethoxyphenylhydrazone; G6P-DH, glucose-6-phosphate dehydrogenase; HK, hexokinase;

HSF, human skin fibroblasts; KCN, cyanide; mGDH, mitochondrial glutamate dehydrogenase; MYXO, myxothiazol; NAO, nonyl acridine orange; N-HSF, human skin fibroblasts with normal karyotype; N-HSF<sub>+DIG</sub>, digitonin-permeabilized human skin fibroblasts with normal karyotype; OLIGO, oligomycin; OXPHOS, oxidative phosphorylation; PKA, protein kinase A; RCI, respiratory control index; ROT, rotenone; SUCC, succinate.

## INTRODUCTION

Trisomy of human chromosome 21 is the most frequent aneuploidy in live births. The clinical entity of trisomy 21 is known as Down syndrome (DS) which affects all major organ systems including the bone, immune, central nervous, muscular and cardiovascular systems [for refs see 1 and 2]. DS is also characterized by premature aging and dementia with neurological features that mimic those found in Alzheimer's disease [3]. Despite a widespread interest in Down syndrome and a vast number of cytogenetic and molecular studies, both the aetiology and the mechanism by which this aneuploidy produces the clinical phenotype and the phenotypic variations are largely unknown. Some studies have indicated the over-expression of genes located on chromosome 21 as the main cause of the complex metabolic derangement in DS [4]. However, other studies have shown how individual loci were not by themselves responsible for specific anatomical, physiological and functional features of the syndrome [5, 6].

A central role for defective mitochondrial functions has been proposed in DS pathogenesis [7], as in other neurodegenerative diseases such as Alzheimer's, Parkinson's and Huntington's diseases [8-10]. Evidence for mitochondrial impairment has been described in various DS cell cultures and tissues. In particular, most studies have analysed gene expression and protein levels of some mitochondrial proteins: down-regulation of genes encoding certain mitochondrial proteins involved in oxidative phosphorylation (OXPHOS) and ATP synthesis have been found in heart of DS foetuses and in amniocytes [11, 12] and increased protein levels of some Krebs cycle enzymes such as aconitase and NADP-linked isocitrate dehydrogenase have been reported in DS brain [13]. However, little is still known about alterations in mitochondria at a functional level: a reduction in some mitochondrial enzyme activities has been reported in platelets from DS patients [14], mitochondrial membrane potential, oxidoreductase activity and mitochondrial morphology are claimed to be altered in DS astrocytes [15] and alteration in mtDNA repair systems has been shown in DS fibroblasts [16]. Although these data are indicative of widespread mitochondrial dysfunctions, the cause of defective mitochondria is still unclear and it remains to be investigated whether and how alterations in pathways/biomolecules of the mitochondrial energy metabolism are involved in the pathogenesis of the syndrome.

In this study, we selectively examined in DS-HSF certain mitochondrial proteins, connected metabolically, that play a role in providing ATP, such as ATPase which catalyses ATP synthesis inside mitochondria, adenine nucleotide translocator (ANT) which causes ATP export from mitochondria in exchange for cytosolic ADP, and adenylate kinase (AK) which catalyses the interconversion of adenylate nucleotides.

We made use of human skin fibroblasts (HSF) from both foetal and adult subjects with chromosome 21 trisomy (DS-HSF) comparing them with euploid fibroblasts (N-HSF) as a suitable cellular model system to explore whether abnormalities in mitochondrial energy metabolism are inherent properties of DS cells; in addition, there is evidence that this peripheral tissue expresses pathophysiological mechanisms relevant for brain dysfunction [17, 18].

We found that both foetal and adult DS-HSF show a drastic reduction in catalytic efficiency for each of the analysed proteins. With the exception of the significant reduction in the amount of ATPase subunits, DS-HSF showed increased levels of ANT and AK but also of other mitochondrial proteins, due to an increase in mitochondrial mass. Furthermore, despite the deficit of mitochondrial ATP production, DS-HSF show no significant change in cellular energy status but increased basal levels of L-lactate, the end product of anaerobic glycolysis, probably as a

compensatory event, together with an increase in mitochondrial mass, to partially offset mitochondrial energy deficit in DS-HFS.

## EXPERIMENTAL

### Cell culture

Five normal and five DS human skin fibroblast cell lines were obtained from the Galliera Genetic Bank (Galliera Hospitals, Genova, Italy). Three DS and three normal fibroblast cultures were established from fetuses spontaneously aborted at a gestational age between 14 and 19 weeks. Two samples each of normal and DS fibroblast cultures were established from donors with trisomic (age 19 and 22 years) and normal (age 30 and 36 years) karyotype. DS and matched normal cell strains were processed and studied in parallel.

The cells were cultured at 37°C in humidified CO<sub>2</sub>/95% air in RPMI 1640 medium (GIBCO/BRL) supplemented with 15% heat-inactivated fetal bovine serum (GIBCO/BRL), 2 mM L-glutamine, penicillin (100 U/ml) and streptomycin (100 µg/ml). Cells were subjected to a 1:2 split every 6 days. Cell protein assay was carried out according to [19]. Comparison of the functional features of normal and DS fibroblasts was made with sub-confluent cultures using a comparable number of culture passages (5-15), in which the growth rate of DS fibroblasts was comparable with that of normal cells; doubling time was about 18 h and 24 h for fetal and non-fetal fibroblasts, respectively.

### Permeabilization of cultured HSF with digitonin

HSF were trypsinized, washed with PBS and suspended in ice-cold sucrose medium consisting of 0.25 M sucrose, 10 mM TRIS-HCl (pH 7.2), 1 mM EGTA, plus 0.01 % digitonin (w/v), as in [20]. After 10 min incubation at ice temperature, cells were centrifuged (150 g for 5 min at 4°C), washed twice with sucrose medium devoid of digitonin, and used for polarographic and spectrophotometric measurements.

Controls were carried out to ensure that plasma membrane permeabilization efficiency with 0.01% digitonin was comparable in both N- and DS-HSF, as shown by measuring the release of L-lactate dehydrogenase in the supernatant after digitonin treatment, as described in [20]. The permeabilization efficiency of HSF was also tested by using the trypan blue dye exclusion test resulting 98-100% in both N- and DS-HSF. Moreover, we confirm that no rupture of the outer mitochondrial membrane occurred in permeabilized HSF: both DS- and N-HSF showed almost 100% outer membrane integrity, assessed as in [21].

### Measurement of oxygen consumption in permeabilized HSF

Oxygen consumption measurements were carried out at 37°C using a Gilson 5/6 oxygraph with a Clark electrode. Digitonin-permeabilized fibroblasts (1 mg) were incubated in 1.5 ml of the respiration medium (210 mM mannitol, 70 mM sucrose, 20 mM TRIS-HCl, 5 mM KH<sub>2</sub>PO<sub>4</sub>/K<sub>2</sub>HPO<sub>4</sub>, pH 7.4, 3 mM MgCl<sub>2</sub>, and 5 mg/ml BSA) with succinate (SUCC; 5 mM) plus 3 µM rotenone (ROT) in the presence (state 3 respiration) or absence (state 4 respiration) of either ADP (0.5 mM) or carbonylcyanide p-trifluoromethoxyphenylhydrazone (FCCP; 1.25 µM).

### Measurement of ANT and AK-dependent mitochondrial ATP efflux

The measurement of ADP/ATP exchange rate via ANT was determined, as described previously in [22], in digitonin-permeabilized fibroblasts incubated at 37°C in 2 ml of the respiration medium described above in the presence of the ATP detecting system (ATP-ds) consisting of glucose (2.5 mM), hexokinase (HK) (2 e.u.), glucose 6-phosphate dehydrogenase (G6P-DH) (1 e.u.) and NADP<sup>+</sup>

(0.25 mM) in the presence of succinate (5 mM) as energy source plus 10  $\mu$ M diadenosine pentaphosphate (Ap5A), used to specifically inhibit AK [23]. NADPH formation in the extramitochondrial phase, which reveals ATP appearance due to externally added ADP (0.5 mM), was monitored as an increase in absorbance at 340 nm. Great care was taken to use enough HK/G6P-DH coupled enzymes to ensure a non-limiting ADP-regenerating system for the measurement of ATP efflux.

Control experiments were carried out as in [22, 24] to ensure that under these experimental conditions OXPHOS-dependent ATP efflux due to externally added ADP was mediated by ANT (see Supplementary data).

The AK activity in digitonin-permeabilized fibroblasts was monitored photometrically at 340 nm in the direction of ATP production by using ADP (0.5 mM) as a substrate in the presence of the ATP-ds described above plus 1  $\mu$ M CAT and 5  $\mu$ M OLIGO used to block ANT and ATP synthase, respectively [22].

It should be noted that the activity of AK that we measured in proliferative permeabilized fibroblasts is thought to be due essentially to the mitochondrial AK isoenzyme since the cytoplasmatic AK isoforms are not expressed in proliferating cells [25].

### Measurement of ATPase activity

Measurements of ATPase activity were carried out in mitochondrial membrane-enriched fractions from cultured HSF. Aliquots of trypsinized HSF cells were washed with ice-cold phosphate-buffered saline, frozen in liquid nitrogen and kept at  $-80^{\circ}\text{C}$  until use. For isolation of mitochondrial membrane-enriched fractions, the pellets were thawed at  $2-4^{\circ}\text{C}$ , suspended in 1 ml of 10 mM TRIS-HCl (pH 7.5), 1mg/ml BSA, and exposed to ultrasound energy for 15 s at  $0^{\circ}\text{C}$ . The ultrasound-treated cells were centrifuged (10 min at 600 g and  $4^{\circ}\text{C}$ ). The supernatant was centrifuged again (10 min at 14000 g and  $4^{\circ}\text{C}$ ) and the resulting supernatant was carefully removed. The pellet was suspended in 1 ml of the respiration medium and ATPase was measured at  $37^{\circ}\text{C}$  by monitoring the OLIGO-sensitive ATP hydrolase activity, essentially as in [26].

### Quantitative real-time PCR

For gene expression measurements, total RNA from normal and DS-HSF cell lines was extracted using the RNeasy plus mini kit (Qiagen). 5  $\mu$ g of total DNA were retrotranscribed by using the reverse transcription Archive Kit (Applied Biosystems<sup>TM</sup>), according to the manufacturer's instructions. The real-time RT-PCR reactions were performed on an Applied Biosystems<sup>TM</sup> 7900HT, as described by the manufacturer. The reaction mixtures contain 2x TM Master Mix Buffer, PDAR System Target 20x FAM (TaqMan<sup>®</sup> Gene Expression Assays), 1  $\mu$ l cDNA template and water. Cycle threshold (Ct) values were obtained graphically, automatically by the instrument, for each gene tested. The glyceraldehyde 3P-dehydrogenase and  $\beta$ -actin housekeeping genes were used as internal standards. Reactions without cDNA were included as a negative control. The relative gene expression for each experiment was calculated using one of five human normal skin fibroblast cell lines as calibrator.

For a quantitative analysis of mtDNA content, total genomic DNA was extracted from normal and DS-HSF cell lines using the NucleoSpin kit (Macherey-Nagel) and real-time PCR reactions were performed on an Applied Biosystems<sup>TM</sup> 7900HT using the SYBR-Green PCR Master Mix (Qiagen). Primers for two mtDNA sequences, D-loop and cytochrome c oxidase II (Cox II), and a nuclear DNA sequence  $\beta$ -actin were used as described in [27]. The reaction mixtures contain 15 ng total genomic DNA, 1X SYBR-Green PCR Master Mix 3.5 mM  $\text{MgCl}_2$  and 0.3  $\mu$ M each primer (Operon Biotechnologies GmbH). Triplicate reactions were performed for each marker in a 96-well plate using a two-step amplification program of initial denaturation at  $95^{\circ}\text{C}$  for 15 min, followed by 35 cycles of  $94^{\circ}\text{C}$  for 20 s and  $61^{\circ}\text{C}$  for 30 s. Standard curves were generated from each experimental plate using serial 5-fold dilutions of genomic DNA.

### Immunoblot analysis

Cell extracts (0.05 mg protein) were loaded onto a 10% SDS-polyacrylamide gel, separated and transferred to a polyvinylidene difluoride membrane which was probed with the following primary antibodies: monoclonal  $\alpha$  subunit of F<sub>1</sub>ATPase (1:250, MitoSciences); monoclonal  $\beta$  subunit of F<sub>1</sub>ATPase (1:400, Santa Cruz); polyclonal d subunit of F<sub>0</sub>ATPase (1:250, Abnova); polyclonal AK2 (1:200, Abgent), polyclonal mGDH (1:1000, provided by Dr. F. Rothe, Institut für Medizinische Neurobiologie, University of Magdeburg, Magdeburg, Germany); polyclonal ANT (1:400, Santa Cruz); monoclonal porin (1:1000, MitoSciences). Immunoblot analysis was performed essentially as described in [28] using horseradish peroxidase-conjugated anti-mouse or anti-rabbit antibodies and enhanced chemiluminescence Western blotting reagents (Amersham, Pharmacia Biotech). Protein levels were normalized using the constitutively expressed  $\beta$ -actin protein using antibody to  $\beta$ -actin (1:500, Sigma Aldrich).

Densitometry values for immunoreactive bands were quantified and protein levels were calculated as a percentage of those in normal fibroblasts taken as 100 in arbitrary units after normalization based on the amount of actin in each lane on the same filter.

### Determination of mitochondrial mass

Mitochondrial mass was determined by using the fluorescent dye 10-*n*-Nonyl-Acridine Orange (NAO; Molecular probes) [29]. Sub-confluent cells were trypsinized and resuspended in 0.5 ml culture medium ( $5 \times 10^5$  cell/ml) supplemented with 25 mM HEPES, pH 7.5 and containing 5  $\mu$ M NAO. After incubation for 10 min at 37°C, cells were spun down, washed with ice-cold medium and transferred immediately to a tube on ice for analysis of the fluorescence intensity by flow cytometry. In each measurement, a minimum of 20,000 cells were analyzed. Data were acquired and analyzed on the FL2 channel using CellQuest software (Becton Dickinson).

### PKA assay and measurement of cellular cAMP levels

The activity of Protein Kinase A (PKA) was measured in cell extracts with cAMP-dependent PKA Assay System (Stressgen), as recommended by the manufacturer. PKA activity was 5-10-fold stimulated by incubation cell extract with 5  $\mu$ M dibutyryl-cAMP (db-cAMP) for 5 min at 37°C.

Intracellular cAMP concentration were measured in cell extracts with cAMP EIA Kit from Stressgen, following the manufacturer's instructions.

### Measurement of cellular adenine nucleotide levels

HSF were trypsinized, washed with PBS and centrifuged at 2000 *g* for 5 min at 4°C. The cellular pellet was subjected to perchloric acid extraction. The amounts of intracellular phosphorylated adenine nucleosides (ATP, ADP, AMP) were determined enzymatically in neutralized extracts as described in [30, 31]. The cellular energy charge ( $\phi$ ) was calculated from the formula:  $([ATP]+1/2[ADP])/([ATP]+[ADP]+[AMP])$  [32].

### Measurement of L-lactate levels

Cells were plated in 5-cm diameter dishes and grown until sub-confluence. 16 h after the culture medium change, the extracellular L-lactate concentration was measured in culture medium by using the L-lactate dehydrogenase method that gives a reliable estimate of L-lactate production inside the cells [33].

### Statistical analysis

Statistical evaluation of the differential analysis was performed by one way ANOVA and Student's t-test. The threshold for statistical significance was set to 0.01.

## RESULTS

### ATP-related mitochondrial metabolism in DS fibroblasts: reduced efficiency of OXPHOS

To investigate whether and how mitochondrial ATP-related metabolism can change in DS fibroblasts, we analysed certain bioenergetic parameters of mitochondria inside cells by comparing trisomic fibroblasts from both spontaneously aborted fetuses and adult donors permeabilized with 0.01 % digitonin (DS-HSF<sub>+DIG</sub>) with respective normal-permeabilized fibroblasts (N-HSF<sub>+DIG</sub>). No differences in permeabilization efficiency and mitochondrial membrane integrity were found between DS-HSF<sub>+DIG</sub> and N-HSF<sub>+DIG</sub> (see Experimental section).

We firstly checked whether changes in oxidative phosphorylation capacity can occur in DS fibroblasts. To do this, we measured mitochondrial respiration inside DS-HSF<sub>+DIG</sub> compared with N-HSF<sub>+DIG</sub> using succinate as an energy substrate. As shown in a typical experiment (Fig. 1A, panels a and b), and in a series of experiments carried out comparing the different DS cell lines with the respective normal cells (Fig. 1B), the ADP-stimulated respiration rate (state 3 respiration) decreased 1.3 ( $\pm$  0.2)-fold in DS-HSF<sub>+DIG</sub> compared to N-HSF<sub>+DIG</sub>, whereas the respiration in the presence of the uncoupler FCCP was equal to the control, indicative of a similar electron flux through Complex II-Complex IV of the respiratory chain.

In spite of a decrease in state 3, a 1.3 ( $\pm$  0.1)-fold increase in state 4 of respiration was found in DS-HSF (Fig. 1B); consistently, the difference between respiration measured in the absence of ADP under non-phosphorylating conditions (+OLIGO) and the residual extra-mitochondrial respiration (+ MYXO), which is indicative of the proton leak [34, 35], was found to be 1.4  $\pm$  0.1-fold greater in DS-HSF<sub>+DIG</sub> compared to N-HSF<sub>+DIG</sub> (see inset of Fig. 1B, panel b).

Respiratory control index (RCI), measured in the presence and absence of ADP or FCCP, was found to be statistically significantly lower in DS-HSF<sub>+DIG</sub> (2  $\pm$  0.2 and 1.4  $\pm$  0.2-fold, respectively) than in respective N-HSF<sub>+DIG</sub> (Fig. 1C), indicating a pronounced decrease in ATP synthesis coupled to substrate oxidation in DS-HSF mitochondria.

No significant differences in these functional features (see panels a of Fig. 1B and 1C) and in all those analyzed below were found among DS (as well as among normal) fibroblasts from fetuses and adult donors.

### ATP-related mitochondrial metabolism in DS fibroblasts: impairment of mitochondrial ATP synthesis machinery

The reduced efficiency of externally added ADP to stimulate the rate of oxygen consumption in DS-HSF mitochondria (Fig. 1) is an indicator of altered OXPHOS capacity which might influence mitochondrial energy production in situ. Thus, to probe further into mitochondrial ATP-related energy production in DS-HSF, we resorted to spectroscopic measurements that allow for the continuous monitoring of ATP synthesised by mitochondria and exported outside cells arising from externally added ADP under conditions in which OXPHOS can occur [30, 22]. To do this, either DS-HSF<sub>+DIG</sub> or N-HSF<sub>+DIG</sub> were incubated in the presence of the ATP detecting system (ATP-ds) and the appearance of ATP outside cells arising from externally added ADP was monitored as an increase in absorbance at 340 nm due to NADPH formation (see panel a of Fig. 2A).

Since in mitochondria ATP efflux can occur with the contribution of both ATPase/ANT activities (in OXPHOS) and AK (which itself, catalyzing the reversible high-energy phosphoryl transfer reaction between adenine nucleosides, can provide ATP from externally added ADP), we used experimental conditions designed to monitor the two pathways separately.

Thus, to selectively measure ATP synthesised via OXPHOS both N-HSF<sub>+DIG</sub> and DS-HSF<sub>+DIG</sub> were treated with Ap5A to inhibit AK [23] (Fig. 2A, panel b): a lower rate of ATP appearance was found in DS-HSF<sub>+DIG</sub> (40% lower than N-HSF<sub>+DIG</sub>), and the addition of CAT plus OLIGO to both N-HSF<sub>+DIG</sub> and DS-HSF<sub>+DIG</sub> almost completely blocked the appearance of ATP.

In the same experiment, when AK-related ATP synthesis was selectively monitored in the presence of CAT plus OLIGO to block OXPHOS (Fig. 2A, panel c), a reduction of about 40% in the rate of ATP synthesis was again found in DS-HSF<sub>+DIG</sub> compared with N-HSF<sub>+DIG</sub>. As expected, the addition of Ap5A to both samples almost completely inhibited the synthesis of ATP.

To ascertain which is the step limiting the rate of ATP synthesis via OXPHOS under our conditions, the application of control strength analysis, performed as in [22, 24], showed that the rate of OXPHOS-dependent ATP production in both N- and DS-HSF reflected that of ADP/ATP exchange mediated by ANT which was found to be impaired in DS-HSF (see Supplementary data).

To gain further insight into the mechanism leading to an ANT deficit in DS-HSF, in a typical experiment (Fig. 2B, panel a), and in a series of experiments carried out comparing the five different DS cell lines with respective normal cells (Table 1), we measured the dependence of the rate of ATP efflux on increasing ADP concentrations in DS-HSF<sub>+DIG</sub> compared with N-HSF<sub>+DIG</sub>. Lineweaver-Burk analysis of data showed a 40% reduction in activity for ANT-mediated ATP efflux in DS-HSF compared to N-HSF, whereas no significant changes were found in the affinity of ANT for the substrate ADP, suggestive of the onset of a non-competitive type of inhibition.

Similarly, kinetic analysis of AK-related ATP synthesis (Fig. 2B, panel b, Table 1) showed a significant reduction in AK activity in DS-HSF compared to N-HSF in spite of unchanged affinity of the enzyme for the substrate ADP.

To verify whether and how alteration to mitochondrial ATPase also occurred in DS-HSF, a direct enzymatic assay of the activity of this protein, estimated as OLIGO-sensitive ATP hydrolase, was carried out in mitochondrial membrane-enriched fraction from DS-HSF and N-HSF (Fig. 3). In a typical experiment, we found a substantial reduction in the rate of ATP hydrolase reaction in DS-HSF with respect to control cells (Fig. 3A). Kinetic analysis (Fig. 3B) revealed a 40% reduction in ATPase activity in DS-HSF compared to N-HSF which was statistically significant ( $p < 0.01$ ) whereas no changes in the affinity of ATPase for the substrate ATP were found (Table 1).

Taken together, these results show a strong impairment of mitochondrial capacity to generate ATP in DS-HSF as a result of a deficit of catalytic efficiency of metabolically-related proteins, such as ANT, ATPase and AK, which play a critical role in supporting energy transfer between ATP-generating and ATP-consuming processes.

### Gene expression and protein levels of ATPase ANT and AK in DS fibroblasts: unchanged gene expression and changes in protein content

Since the reduction in ATPase ANT and AK activities found in DS-HSF could also be the result of changes in their gene expression and/or in the protein content, we investigated both the gene expression and protein levels of certain protein subunits from ATPase, AK2, the AK isoform expressed in the mitochondrial intermembrane space [25], and ANT2, the ANT isoform mainly expressed in fibroblasts [36]. As a control, the levels of gene and protein expression of glutamate dehydrogenase (mGDH), a matrix mitochondrial enzyme, were also measured.

When gene expression was analyzed by real-time RT-PCR in DS and normal samples (Fig 4A), no significant differences in *ATP5A* (encoding the  $\alpha$  subunit of F<sub>1</sub>ATPase), *ATP5B* (encoding the  $\beta$  subunit of F<sub>1</sub>ATPase), *AK2* (encoding isoform 2 of AK), *SLC25A5* (encoding isoform 2 of ANT) and *GLUD1* (encoding mGDH) gene expression were found in DS-HSF compared with N-HSF ( $p > 0.02$ ).

When protein levels were analyzed by immunoblotting analysis in HSF homogenates obtained from DS and normal samples (Fig 4B, panel a), densitometric analysis revealed a decrease in all ATPase subunits analysed i.e. the  $\alpha$  and  $\beta$  subunit of F<sub>1</sub>ATPase (16 %  $\pm$  4 and 15%  $\pm$  5) and subunit d of F<sub>0</sub>ATPase (20%  $\pm$  4) (Fig. 4B, panel b). Surprisingly, in spite of the strong reduction in their

activities (see Fig. 3), the amount of both AK2 and ANT2 proteins was found to increase ( $30\% \pm 3$  and  $27\% \pm 2.6\%$ , respectively) in DS-HSF. A similar increase in the mitochondrial matrix enzyme mGDH, and the structural mitochondrial protein porin content was also found in DS-HSF compared with normal cells.

These results indicate a shared pattern of increase in levels of all mitochondrial proteins tested in DS samples with the exception of the ATPase subunits. However, if we compare the mitochondrial protein/porin ratios for DS-HSF and N-HSF, the decrease in the level of ATPase subunits is more significant (about 35%), whereas no changes were obtained for the other mitochondrial proteins, thus indicating a selective down-regulation of the ATPase protein in DS cells.

Interestingly, the treatment of DS-HSF cultures with a cocktail of protease inhibitors did completely rescue the protein level of all ATPase subunits analyzed (Fig. 4C).

### Involvement of cAMP/PKA pathway in ATPase, ANT and AK deficit

If proteolytic degradation events of ATPase protein could explain the deficit of ATPase activity found in DS-HSF, to give some insight into the cause of ANT and AK impairment, despite no reduction in their protein levels, we tested the hypothesis that changes in signalling pathways, such as cAMP/protein kinase A (PKA) could be involved in ANT, AK and ATPase deficit found in DS-HSF. In this regard, it has been shown that the Ts65Dn mouse model of DS exhibits altered signalling pathways which involve, among others, cAMP-dependent PKA activity as a result of decreased basal levels of cAMP [37]. We measured the cellular pool of cAMP as well as PKA activity in HSF revealing a significant decrease in DS-HSF for both the basal level of cAMP (about 30 % that found in N-HSF, Fig. 5A) and PKA activity (about 60 % that measured in N-HSF, Fig. 5B). Furthermore, PKA activity was found to be activated by short-time incubation with db-cAMP, a permanent derivative of cAMP, in DS-HSF as well as normal cells.

Interestingly, exposure of DS-HSF to db-cAMP completely prevented the deficit of ANT and AK activities and partially that of ATPase activity in DS-HSF. The involvement of the PKA pathway in the cAMP-dependent activation of the investigated proteins was further demonstrated by the ability of H89, a specific inhibitor of PKA [38], to prevent activation of ATPase, ANT and AK activities when incubated with the cells, before adding db-cAMP (Fig. 5C).

As for ATPase, when DS-HSF cultures were treated with both protease inhibitors and db-cAMP, the rescue of ATPase activity was almost complete (Fig. 5C, panel a) suggesting an involvement of both the events i.e. selective ATPase degradation and cAMP/PKA-dependent pathway in regulating ATPase activity in DS-HSF.

### Increase in mitochondrial mass in DS fibroblasts

To ascertain whether the almost general increase in the amount of mitochondrial proteins found in DS-HSF was due to an increase in mitochondrial mass, we used the fluorescent dye nonyl acridine orange (NAO) to label mitochondria, and mitochondrial mass was monitored by flow cytometry (Fig. 6). As a control, the effect of the uncoupler FCCP ( $1.25 \mu\text{M}$ ) was determined, resulting in a transmembrane potential-independent staining of mitochondria (data not shown). As shown in a typical experiment (Fig. 6, panel a), the relative NAO intensity was found to increase as compared with normal cells in a statistically significant manner ( $25\% \pm 1$ ;  $p < 0.01$ ) in five different DS and N samples (Fig. 6, panel b), thus indicating that an increase in mitochondrial mass occurs in DS-HSF.

To confirm this, we measured mtDNA content of both DS- and N-HSF by real-time PCR analysis. As shown in Fig. 6B, the mtDNA content was 2-fold higher in DS cells than that measured in normal HSF. This increase in mtDNA content was consistent with the increase in mitochondrial mass found in DS-HSF, as revealed by NAO staining.

### Cell energy status in DS fibroblasts

To investigate whether the impairment of mitochondrial ATP production found in DS-HSF could influence cell energy status, we measured the cellular adenine nucleotide pool (ATP, ADP and AMP) in both DS and normal HSF (Table 2). ATP, ADP and AMP were only slightly reduced in DS-HSF compared with normal cells. Therefore, the cell energy charge, a sensitive indicator of cell energy status [32], does not significantly change in DS as compared to normal cells.

In order to understand how cellular ATP content is only slightly reduced in DS-HSF in spite of the strong impairment of mitochondrial ATP synthesis machinery (see Figs. 1-3), we investigated whether pathways alternative to OXPHOS contribute to energy demand in DS-HSF. Given that glycolytic substrate-level phosphorylation is the major alternative pathway providing ATP, and that its final step is the cytosolic conversion of pyruvate to L-lactate, we measured both ATP and L-lactate content in DS-HSF and N-HSF (Fig. 7).

Consistently with a strong impairment of mitochondrial ATP production in DS, the cellular level of ATP was drastically lower in DS-HSF than in normal cells when fibroblasts were grown in a galactose medium in the absence of glucose (Fig 7A), a condition in which ATP is essentially produced by mitochondrial OXPHOS [39]. Thus, without glucose, DS-HSF show to be strongly defective in ATP production. Conversely, in a glucose cultivation medium in the presence of 5  $\mu$ M OLIGO, already found to completely inhibit OXPHOS-dependent ATP synthesis (see Fig 2A), the ATP level in DS cells was higher than in control.

Consistently with a compensatory enhancement of glycolysis, levels of L-lactate were found to be higher in DS-HSF ( $45\% \pm 3$ ) with respect to N-HSF under basal conditions (i.e. without OLIGO) (Fig. 7B). In the presence of OLIGO, as expected, the L-lactate pool in N-HSF was found to increase by 40% compared with that measured in the absence of OLIGO, whereas in DS cells L-lactate production increased in the presence of OLIGO by only about 15% of that found in the absence of the ATPase inhibitor.

These results show that a significant shift from oxidative phosphorylation to glycolytic substrate-level phosphorylation occurs in DS cells to meet the cellular demand for ATP.

## DISCUSSION

In the present study, we dissect in some detail certain individual steps involved in mitochondrial ATP production in human skin fibroblasts with chromosome 21 trisomy, providing new insight into the molecular basis for mitochondrial dysfunction in Down syndrome.

Since foetal fibroblasts and fibroblasts established from donors with DS show comparable alterations in the mitochondrial features investigated, we argue that the energy competent modification of DS fibroblasts is an inherent feature of these cells per se and likely to be already established before birth.

We report here a detailed functional study which gives direct evidence of a deficit of mitochondrial ATP synthesis machinery and provide new information on cell energy status in DS fibroblasts. We show for the first time that DS cells had a decreased efficiency of the mitochondrial energy production apparatus, selectively involving the ADP/ATP translocator, ATP synthase, and adenylate kinase (Figs. 1-3).

The reduction in respiratory control index of mitochondria within cells in DS-HSF gives an indication of alterations of catalytic oxidative phosphorylation capacity [36], whereas the respiratory capacity was unaffected in DS-HSF, as shown by the FCCP-stimulated succinate respiration comparable to control fibroblasts (Fig. 1). Another indication of non optimal efficiency of OXPHOS is an increase in respiration of DS fibroblasts when in situ mitochondria were in non phosphorylating condition, (Fig. 1B), suggestive of a greater proton leak across the inner mitochondrial membrane [40].

We confirmed the decrease in ATP synthesis coupled to substrate oxidation by experiments in which we directly measured ATP export outside mitochondria following external addition of ADP to permeabilized HSF under conditions in which oxidative phosphorylation can occur: we found a drastic decrease in the rate of ATP efflux in DS-HSF (Fig. 2A, panel b).

Kinetic analysis of ANT-dependent ATP efflux, AK activity and ATP hydrolase-catalyzed reaction revealed a severe reduction in transport efficiency of ANT and in the catalytic efficiency of both ATPase and AK in spite of unchanged affinity for their substrates, providing further insight into the mechanism by which mitochondrial ATP synthesis is impaired in DS-HSF.

The deficit of ANT as well as of AK activity in DS fibroblasts is particularly interesting because it occurred even though both the proteins were not only not differentially expressed (Fig. 4A), but up-regulated at the protein level (Fig. 4B); thus, we assume that the impairment of their activity could be caused by post-translational modification.

In the case of ATPase, the decrease in ATPase subunits found completely rescued in DS-HSF after treatment with protease inhibitors, revealed an enhanced specific proteolytic cleavage of the enzyme complex.

We hereby give indications aiming to account for the deficit of AK, ANT and ATPase activities found in DS fibroblasts. In agreement with the decrease in both cellular cAMP level and PKA activity found in DS-HSF (Fig. 5A and 5B), we showed that ANT, AK and ATPase activities were restored by short-term incubation with db-cAMP, which strongly increases PKA activity, this cAMP promoting effect being completely suppressed by the PKA inhibitor H89 (Fig 5C). Thus, in DS-HSF, the effect of cAMP on mitochondrial protein activities involves PKA. The cAMP/PKA-dependent restoring of ANT, AK and ATPase deficit is consistent with a recent study reporting that cAMP regulates mitochondrial ATP production through PKA-mediated cAMP-dependent phosphorylation of mitochondrial proteins involved in mitochondrial ATP synthesis [41]. Further studies are in progress to clarify this aspect.

Our results strongly suggest that in DS cells the decrease in PKA activity as a result of decreased basal levels of cAMP, could cause alterations in cAMP-dependent PKA signalling pathway and then post-translational cAMP/PKA mediated alteration of the catalytic activity of the analyzed mitochondrial proteins.

We also found that DS-HSF displayed a significantly enhanced mitochondrial mass and mtDNA (Fig. 6). An increase in mitochondrial mass and mtDNA copy number of cells has also been observed in fibroblasts during replicative cell senescence associated with a decline in mitochondrial respiratory function [42]. Consistently, our results showed an increase in mitochondrial mass in DS fibroblasts with impaired mitochondrial energy system. Thus, the increase in mitochondrial mass in DS-HSF could be one of the factors involved in feedback compensation, due to the deficit of mitochondrial functions in DS cells. However, the increase in mitochondrial mass did not fully compensate for the impairment of mitochondrial ATP synthesis machinery which remained 40-45% lower in DS cells although mitochondrial mass was found to increase by 25% in DS-HSF compared to N-HSF to compensate for an impairment which would otherwise be more striking.

In spite of a reduced ability of DS cells to synthesize ATP by oxidative phosphorylation, ATP levels in DS cells were only slightly reduced in DS-HSF compared with normal cells and the cellular energy charge, a regulator parameter of the adenylate pool controlling the energy metabolism, was not significantly different in DS fibroblasts compared with normal cells (Table 2).

An answer to the question as to how ATP production is maintained essentially constant in DS cells is given by the D-glucose to galactose switch assay, which disables glycolysis, and by L-lactate measurements. A strict requirement for extracellular glucose to maintain intracellular ATP levels, an oligomycin-insensitive cellular ATP production and an increase in basal levels of L-lactate in DS fibroblasts (Fig. 7) demonstrates that DS cells, in which OXPHOS is physiologically impaired, rely mainly on glycolytic ATP production for their energy demands.

In conclusion, our study identifies new molecular targets for mitochondrial dysfunction in DS which could play a role in DS pathogenesis: DS cells show an impairment of OXPHOS capacity involving ATPase, ANT and AK deficit, events which might be ascribed to post-translational activities. A novel feature is shown here for DS fibroblasts, in that they partially compensate for mitochondrial energy deficit by increasing glycolysis and mitochondrial mass, thus partly offsetting potential energy damage for the cell.

As for the implications of our results for Down syndrome, the identification of molecular targets responsible for OXPHOS deficiency in DS cells might provide a molecular explanation for some clinical phenotypic features of the syndrome. Indeed, mitochondrial or nuclear genetic defects involving enzymes of OXPHOS machinery are characterized by clinical manifestations including developmental delay, hypotonia, ophthalmoplegia, muscle weakness, cardiomyopathy and lactacidosis, [43], clinical signs present, albeit with a variable severity, also in DS subjects [44].

### **Acknowledgements**

The linguistic review of this manuscript by Anthony Green is gratefully acknowledged.

We thank the Galliera Genetic Bank – Network of Telethon Genetic Biobanks project GTB07001 for providing us with fibroblast cell lines.

This work was partially supported by a grant “Molecular determinants and mitochondrial bioenergetics in Down syndrome” from “Fondation Jérôme Lejeune” (to RAV) and by Italian Ministry of Instruction, University and Research (MIUR)-Programmi di Ricerca Scientifica di Rilevante Interesse Nazionale (PRIN) project 2008FHM37R\_002 (to RAV).



20. Ouhabi, R., Boue-Grabot M. and Mazat, J. P. (1998) Mitochondrial ATP synthesis in permeabilized cells: assessment of the ATP/O values *in situ*. *Anal. Biochem.* **263**, 169-175.
21. Kuznetsov, A. V., Veksler, V., Gellerich, F. N., Saks, V., Margreiter, R. and Kunz, W. S. (2008) Analysis of mitochondrial function *in situ* in permeabilized muscle fibers, tissues and cells. *Nature Protocols* **3**, 965-976.
22. Valenti, D., Vacca, R. A., de Pinto, M. C., De Gara, L. Marra, E. and Passarella, S. (2007) In the early phase of programmed cell death in Tobacco Bright Yellow 2 cells the mitochondrial adenine nucleotide translocator, adenylate kinase and nucleoside diphosphate kinase are impaired in a reactive oxygen species-dependent manner. *Biochem. Biophys. Acta* **1767**, 66-78.
23. Lienhard, G. E. and Secemski, I. I. (1973) P<sub>1</sub>P<sub>5</sub>-Di(adenosine-5')pentaphosphate, a potent multisubstrate inhibitor of adenylate kinase. *J. Biol. Chem.* **248**, 1121-1123.
24. Atlante, A., Bobba, A., de Bari, L., Fontana, F., Calissano, P., Marra, E. and Passarella, S. (2006) *J. Neurochem.* **97**, 1166-1181.
25. Noma, T. (2005) Dynamics of nucleotide metabolism as a supporter of life phenomena. *J. Med. Invest.* **52**, 127-136.
26. Bénit P., Goncalves, S., Philippe Dassa, E., Brière, J. J., Martin, G. and Rustin, P. (2006) Three spectrophotometric assays for the measurement of the five respiratory chain complexes in minuscule biological samples. *Clin. Chim. Acta* **374**, 81-86.
27. Chen, J., Kadlubar, F. F. and Chen, J.Z. (2007) DNA supercoiling suppresses real-time PCR: a new approach to the quantification of mitochondrial DNA damage and repair. *Nucleic Acids Res.* **35**, 1377-1388.
28. Vacca, R. A., Marra, E., Loverro, G., Maiorano, E., Napoli, A., Lovecchio, M., Selvaggi, L. and Perlino, E. (2003) Differential expression of beta 1c integrin messenger ribonucleic acid and protein levels in human endometrium and decidua during the menstrual cycle and pregnancy. *J. Clin. Endocrinol. Metab.* **88**, 720-729.
29. Maftah A., Petit, J. M., Ratinaud, M. H. and Julien, R. (1989) 10-N nonyl-acridine orange: a fluorescent probe which stains mitochondria independently of their energetic state. *Biochem. Biophys. Res. Commun.* **164**, 185-190.
30. Passarella, S. Ostuni, A., Atlante, A. and Quagliariello, E. (1988) Increase in the ADP/ATP exchange in rat liver mitochondria irradiated *in vitro* by helium-neon laser. *Biochem, Biophys, Res, Commun.* **156**, 978-986.
31. Jebens, E. and Sejersted, O. M. (1992) Enzymatic microdetermination of plasma and serum free fatty acid. *Scand. J. Clin. Lab. Invest.* **52**, 714-724.
32. Atkinson, D. E. (1968) The energy charge of the adenylate pool as a regulatory parameter. Interaction with feedback modifiers. *Biochemistry* **7**, 4030-4034.
33. Walz, W. and Mukerji, S. (1988) Lactate production and release in cultured astrocytes, *Neurosci. Lett.* **86**, 296-300.
34. Markley, M. A., Pierro, A. and Eaton, S. (2002) Hepatocyte mitochondrial metabolism is inhibited in neonatal rat endotoxaemia: effects of glutamine. *Clin. Sci.* **102**, 337-344.
35. Gnaiger, E. (2009) Mitochondrial respiratory control. In *Textbook on Mitochondrial Physiology* (Gnaiger, E., ed.) Mitochondr. Physiol. Soc. electronic ed.
36. Doerner, A., Pauschinger, M., Badorff, A., Noutsias, M., Giessen, S., Schulze, K., Bilger, J., Rauch, U. and Schultheiss, H. P. (1997) Tissue-specific transcription pattern of the adenine nucleotide translocase isoforms in humans. *FEBS Lett.* **414**, 258-262.
37. Siarey, R. J., Kline-Burgess, A., Cho, M., Balbo, A., Best, T. K., Harashima, C., Klann, E. and Galdzicki, Z. (2006) Altered signalling pathways underlying abnormal hippocampal synaptic plasticity in the Ts65Dn mouse model of Down syndrome, *J. Neurochem.* **98**, 1266-1277.
38. Chijiwa, T., Mishima, A., Hagiwara, M., Sano, M., Hayashi, K., Inoue, T., Naito, K., Toshioka, T. and Hidaka, H. (1990) Inhibition of forskolin-induced neurite outgrowth and protein phosphorylation by a newly synthesized selective inhibitor of cyclic AMP-dependent protein kinase, N-[2-(p-bromocinnamylamino)ethyl]-5-isoquinolinesulfonamide (H-89), of PC12D pheochromocytoma cells. *J. Biol. Chem.* **265**, 5267-5272.

39. Rossignol, R., Gilkerson R., Aggeler, R., Yamagata, K., Remington, S. J. and Capaldi, R. A. (2004) Energy substrate modulates mitochondrial structure and oxidative capacity in cancer cells. *Cancer Res.* **64**, 985-993.
40. Buttergereit, F. and Brand, M. D. (1995) A hierarchy of ATP-consuming processes in mammalian cells. *Biochem. J.* **312**, 163-167).
41. Acin-Perez, R., Salazar, E., Kamenetsky, M., Buck, J., Levin, L. R. and Manfredi, G. (2009) Cyclic AMP produced inside mitochondria regulates oxidative phosphorylation, *Cell Metab.* **9**, 265-276.
42. Lee, H. C., Yin, P. H., Chi, C. W. and Wei, Y. H. (2002) Increase in mitochondrial mass in human fibroblasts under oxidative stress and during replicative cell senescence, *J. Biomed. Sci.* **9**, 517-526.
43. Gibson, K., Halliday, J. L., Kirby, D. M., Yapfite-Lee, J., Thorburn, D. R. and Boneh, A. (2008) Mitochondrial Oxidative Phosphorylation Disorders Presenting in Neonates: Clinical Manifestations and Enzymatic. *Pediatrics* **122**, 1003-1008.
44. Epstein, C.J. (1995) Down syndrome. In: *The metabolic and molecular bases of inherited diseases* (Scriver, C. R., Beaudet, A. L., Sly, W. S., Valle, D. eds) 7<sup>th</sup> Edition, Vol I New York: McGraw, Inc., pp 749-794.

**Table 1****Kinetic parameters of ANT, AK and ATPase in DS-HSF.**

Enzymes	N-HSF (n=5)		DS-HSF (n=5)	
	$V_{\max}$ (nmol/min / mg protein)	$K_m$ ( $\mu$ M)	$V_{\max}$ (nmol/min / mg protein)	$K_m$ ( $\mu$ M)
ANT <sup>a</sup>	28 $\pm$ 4	5 $\pm$ 3	16 $\pm$ 4*	6 $\pm$ 2
AK <sup>a</sup>	85 $\pm$ 5	58 $\pm$ 4	50 $\pm$ 4*	60 $\pm$ 3
ATPase <sup>b</sup>	50 $\pm$ 5	17 $\pm$ 2	30 $\pm$ 5*	18 $\pm$ 1

<sup>a</sup>The enzyme activities were measured in digitonin-permeabilized fibroblasts (1 mg protein) under experimental conditions described in the legend of Fig. 2A.

<sup>b</sup>The enzyme activity was measured in mitochondrial membrane-enriched fractions (0.1 mg protein) under experimental conditions described in the legend of Fig. 3A.

Values represent the means  $\pm$  SEM of three experiments on cell cultures from the five different controls and the five different DS cell lines. \*Statistically significantly different with  $p < 0.01$  when comparing N and DS samples.

**Table 2****Adenine nucleotide content in DS-HSF.**

	ATP	ADP	AMP	$\Phi^a$
<b>Cell type</b>	Nucleotide content (nmol/mg cell protein)			
N-HSF (n=5)	12.5 ± 0.45	2.3 ± 0.14	2.7 ± 0.12	0.78 ± 0.02
DS-HSF (n=5)	10.5* ± 0.40	2.0* ± 0.16	2.3* ± 0.10	0.78 ± 0.01

<sup>a</sup> $\Phi = ([ATP] + 1/2[ADP]) / ([ATP] + [ADP] + [AMP])$ .

The values are the means ± SEM of three experiments on cell cultures from the five different controls and the five different DS cell lines. \*Statistically significantly different with  $p < 0.01$  when comparing N and DS samples.

## Figure legends

**Fig. 1. Respiratory capacity of DS-HSF.** (A) N-HSF<sub>+DIG</sub> (panel a) and DS-HSF<sub>+DIG</sub> (panel b) (1 mg protein each) were incubated at 37°C in 1.5 ml of respiration medium and oxygen consumption was measured polarographically as a function of time. Where indicated, 5 mM SUCC, 0.5 mM ADP, 5 µM OLIGO, 1.25 µM FCCP and 2.5 µM AA were added. The rate of oxygen consumption is expressed as ng-atoms O/min x mg protein. (B) The rate of oxygen consumption was measured in either state 4 (in the presence of 5 mM SUCC) or state 3 respiration (in the presence of 5 mM SUCC plus 0.5 mM ADP or 1.25 µM FCCP). Panel a reports the means (± SEM) of three different experiments on each normal (foetal, ○ and adult, Δ) and corresponding trisomic (foetal, ● and adult, ▲) cell line. Panel b reports the statistical analysis (± SEM) of experiments performed on all five normal and corresponding five trisomic cell lines. The inset shows the rate of oxygen consumption measured in both N- and DS<sub>+DIG</sub> in the presence of either oligomycin (12 µg/mg of protein) (+OLIGO) or myxothiazol (3 µg/mg of protein) (+MYXO) and the difference between oxygen consumption of HSF in the presence of OLIGO and that measured in the presence of MYXO (OLIGO-MYXO). (C) RCI, measured ± ADP or ± FCCP, is reported as the means (± SEM) of three different experiments on each normal (foetal, ○ and adult, Δ) and trisomic (foetal, ● adult, ▲) cell line (panel a) and as statistical analysis performed on all five normal and the corresponding five trisomic cell lines (panel b). Significant differences between N and DS samples are indicated with asterisks (\* =  $p < 0.01$ ; \*\* =  $p < 0.001$ ).

**Fig. 2. ATP efflux due to externally added ADP in HSF.** (A) Scheme (panel a) represents the ATP detecting system. For details see text; IMS, inter membrane space; IM, mitochondrial inner membrane; OM, mitochondrial outer membrane. Both N-HSF<sub>+DIG</sub> and DS-HSF<sub>+DIG</sub> (1 mg protein each) were incubated at 37°C in 2 ml of respiration medium in the presence of the ATP-ds plus 5 mM SUCC with either 1 µM CAT plus 5 µM OLIGO (panel b) or 10 µM Ap5A (panel c); where indicated, ADP (0.5 mM) was added. Numbers along curves are rates of absorbance increase at 340 nm measured as tangents to the initial slopes and expressed as nmol NADP<sup>+</sup> reduced/min/mg cellular protein. (B) Lineweaver-Burk analysis of ANT- and AK-dependent ATP efflux. ADP was added at the indicated concentrations to either N-HSF<sub>+DIG</sub> or DS-HSF<sub>+DIG</sub> (1 mg protein, each) and the inverse of the rate of ANT-dependent ATP efflux (panel a) and of AK-dependent ATP synthesis (panel b) were plotted versus the inverse of the ADP concentration.

**Fig. 3. ATPase activity in HSF mitochondria.** (A) ATPase-dependent ATP hydrolysis was measured on mitochondrial membrane-enriched fractions obtained from both N-HSF and DS-HSF (0.1 mg protein each) incubated at 37°C in 1 ml of respiration medium. Where indicated, 0.2 mM NADH, 8 µM ROT, 3 mM KCN were added. At the arrow, the reaction started by addition of a mixture (MIX) containing 2 mM PEP, 0.5 mM ATP and the coupled enzymes PK-L-LDH (2 e.u.). Where indicated, 5 µM OLIGO was added. Numbers along curves are rates of absorbance decrease at 340 nm, measured as tangents to the initial slopes and expressed as nmol NADH oxidised/min x mg mitochondrial protein. (B) Lineweaver-Burk analysis of ATPase-catalysed ATP hydrolysis. ATP was added at the indicated concentrations to mitochondrial membrane-enriched fractions of N-HSF and DS-HSF (0.1 mg protein, each) and the inverse of the rate of ATP hydrolysis was plotted versus the inverse of ATP concentration.

**Fig. 4. Gene expression and protein levels of ATPase subunits, ANT2 and AK2 in HSF.** (A) Gene expression of *ATP5A*, encoding the α subunit of F<sub>1</sub>-ATPase, *ATP5B*, encoding the β subunit of F<sub>1</sub>-ATPase, *AK2*, encoding AK isoform 2, *SLC25A5*, encoding ANT isoform 2 and *GLUD1* encoding the mitochondrial matrix enzyme mGDH, were measured by real-time RT-PCR in DS- and N-HSF. Gene levels were expressed in arbitrary units (A.U.) after normalization with β-actin

using one human normal skin fibroblast cell line as calibrator. The values are reported as the means ( $\pm$  SEM) of experiments performed on five normal and five trisomic cell lines. **(B)** Protein levels of  $\alpha$  and  $\beta$  subunits of F1-ATPase, subunit d of Fo-ATPase, AK isoform 2 (AK2) and ANT isoform 2 (ANT2) were measured by immunoblot analysis (**panel a**) of cell extracts (0.05 mg protein) of DS- and N-HSF using the respective antibodies; protein levels of mGDH and porin, as mitochondrial protein markers and actin as cytosolic protein marker were also measured. For each protein, values are reported, after densitometric analysis and normalization with  $\beta$ -actin, (**panel b**) as the means ( $\pm$  SEM) of experiments performed on five normal and five trisomic cell lines. For each cell line, the measurements were performed in triplicate. The data are expressed as a percentage of those in normal cells. Significant differences between N and DS samples are indicated with asterisks ( $* = p < 0.01$ ). **(C)** Where indicated, HSF were treated for 48 h with the protease inhibitor cocktail (SIGMA) at a dilution of 1:400 (**+PI**). Protein levels of  $\alpha$  and  $\beta$  subunits of F1-ATPase and subunit d of Fo-ATPase were measured in cell extracts (0.05 mg protein) of DS- and N-HSF by immunoblot analysis using the respective antibodies (**panel a**). For each protein, values are reported, after densitometric analysis and normalization with  $\beta$ -actin, as a percentage of those in normal cells (**panel b**).

**Fig. 5. Cellular levels of cAMP, PKA activity and effect of db-cAMP and H89 on ATPase, ANT and AK activities in DS-HFS.** **(A)** Cellular levels of cAMP were determined in fibroblasts as described in Experimental section. **(B)** PKA activity was measured in cell lysate as described in Experimental section and reported as percentage of normal cells. Significant differences between N and DS samples are indicated with asterisks ( $** = p < 0.001$ ). **(C)** Where indicated, DS-HSF were incubated for 2 h in the presence of 100  $\mu$ M db-cAMP (**+cAMP**), or preincubated 2h with H89 (50  $\mu$ M) before adding db-cAMP (**H89+cAMP**). ATPase (**panel a**), ANT (**panel b**) and AK (**panel c**) activities were determined as described in Experimental section and expressed as a percentage of those in normal cells. For ATPase activity measurement, cells were treated for 48 h with the protease inhibitor cocktail (SIGMA) at a dilution of 1:400 (**+PI**) or treated with both PI and db-cAMP (**+PI+cAMP**). Variation among treated and non-treated normal cells was less than 10 %. The data represent means ( $\pm$  SEM) for experiments performed on five normal and five trisomic cell lines. Significant differences between DS-treated and non-treated samples are indicated with asterisks ( $* = p < 0.01$ ;  $** = p < 0.001$ ).

**Fig 6. Mitochondrial mass and mtDNA content in HFS.** **(A)** Cells were stained with NAO and the mitochondrial mass was measured by flow cytometry (**panel a**). The area under the continuous curve represents the population of normal cells, and the area under the dashed curve represents the population of DS cells. The mean values ( $\pm$  SEM) of mitochondrial mass, expressed as percentage of NAO fluorescence in normal cells, obtained from three different experiments on five normal and five DS cell lines are reported in **panel b**. **(B)** mtDNA content was assayed using real-time PCR. Two mtDNA markers (D-loop and Cox II) and a nuclear DNA marker ( $\beta$ -actin) were used. The relative amplification of mtDNA markers in DS fibroblasts versus normal cells was calculated upon normalization to the reference  $\beta$ -actin as described in Materials and Methods. Values are the mean  $\pm$  S.E. of three independent experiments on five normal and five DS cell lines. Significant differences between N and DS samples are indicated with asterisks ( $** = p < 0.001$ ).

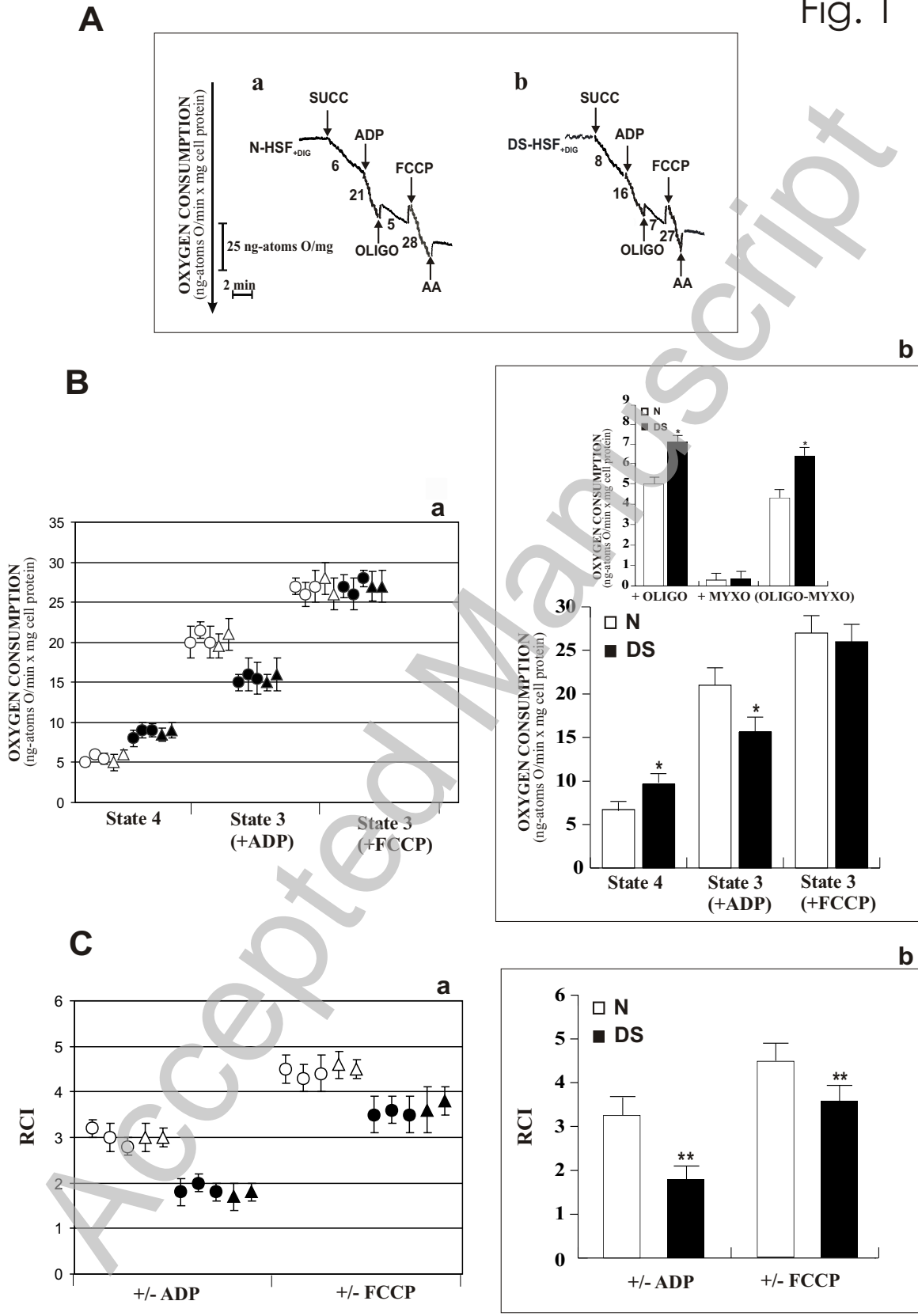
**Fig. 7. Steady state levels of ATP and L-lactate in HSF: effect of glucose withdrawal and oligomycin.** **(A)** Cells were cultured for 48 h in a medium without glucose and supplemented with either 10 mM galactose (Gal) or 10 mM glucose (Glu). Where indicated, cells were incubated for 16 h with 5  $\mu$ M OLIGO (**+OLIGO**). Cellular ATP content was measured as detailed in Experimental section and reported as a percentage of that in normal cells grown in the presence of 10 mM glucose. **(B)** Cells were incubated for 16 h in the absence (**-OLIGO**) or in the presence of 5  $\mu$ M OLIGO (**+OLIGO**). The level of L-lactate was measured in culture medium (see Experimental section) and reported as a percentage of that in normal cells.

The data represent means ( $\pm$  SEM) for experiments performed on five normal and five trisomic cell lines. For each cell line the measurements were performed in triplicate. All samples were statistically significantly different (\* =  $p < 0.01$ ; \*\* =  $p < 0.001$ ) when comparing N with the respective DS samples.

Accepted Manuscript

THIS IS NOT THE VERSION OF RECORD FOR THE JOURNAL. See the journal website for the final version.

Fig. 1



THIS IS NOT THE VERSION OF THE MANUSCRIPT. PUBLISHED ON 10 AUG 2010 AS MANUSCRIPT BJ20100581

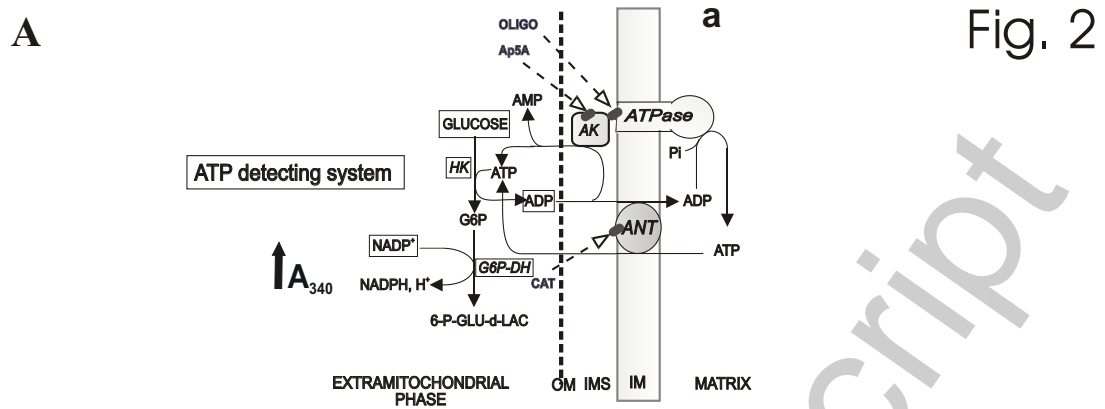
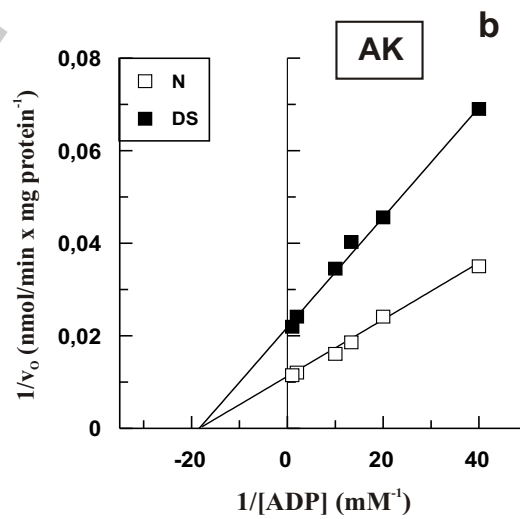
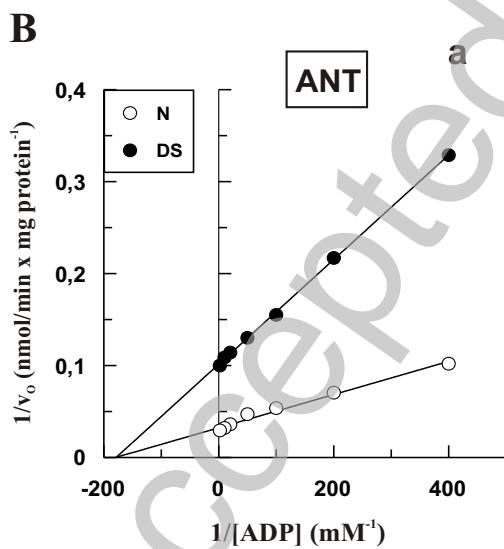
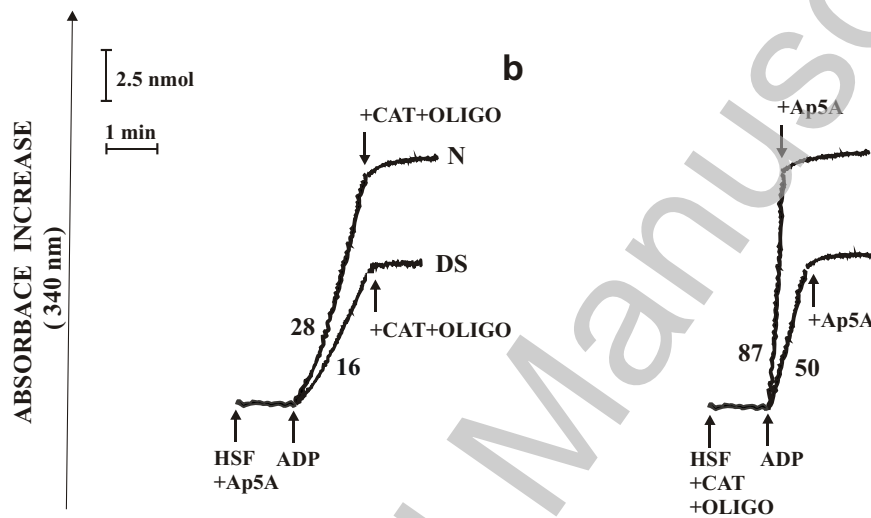
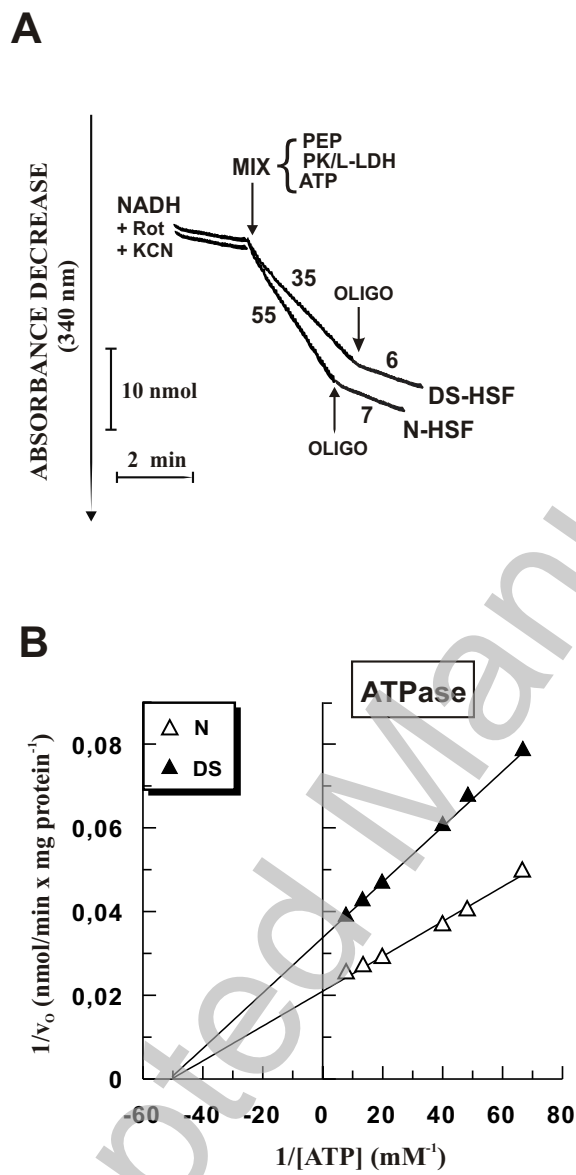


Fig. 2



THIS IS NOT THE VERSIION OF THE MANUSCRIPT. PUBLISHED ON 10 AUG 2010 AS MANUSCRIPT BJ20100581

Fig. 3



THIS IS NOT THE VERSION OF THE MANUSCRIPT. PLEASE REFER TO THE ORIGINAL MANUSCRIPT FOR THE CORRECT VERSION.

Accepted Manuscript

Fig. 4

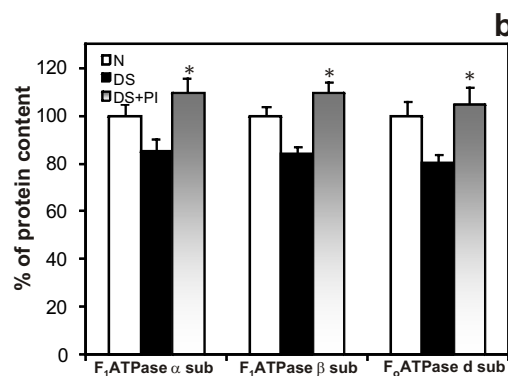
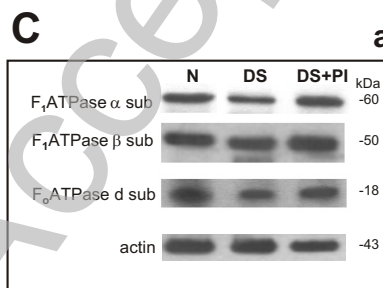
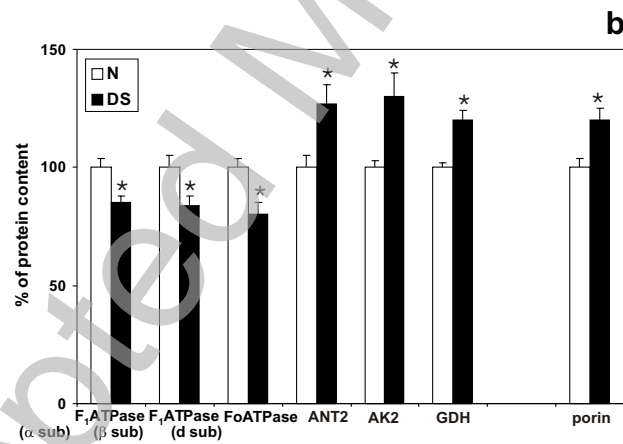
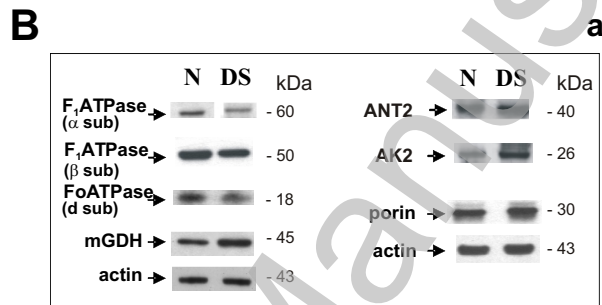
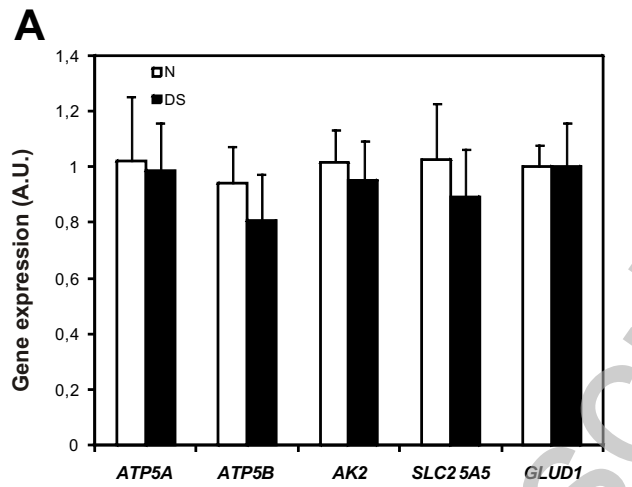


Fig. 5

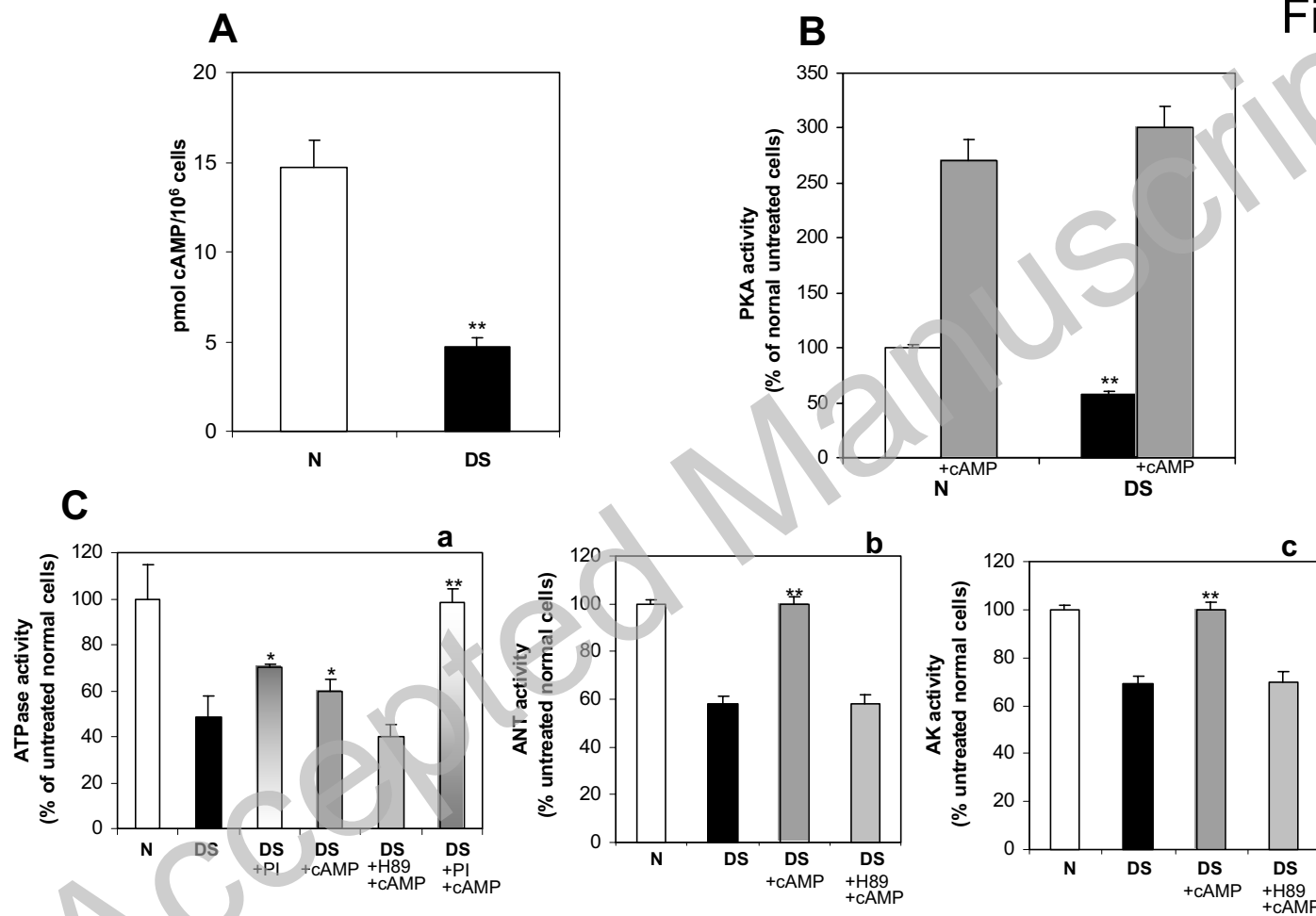
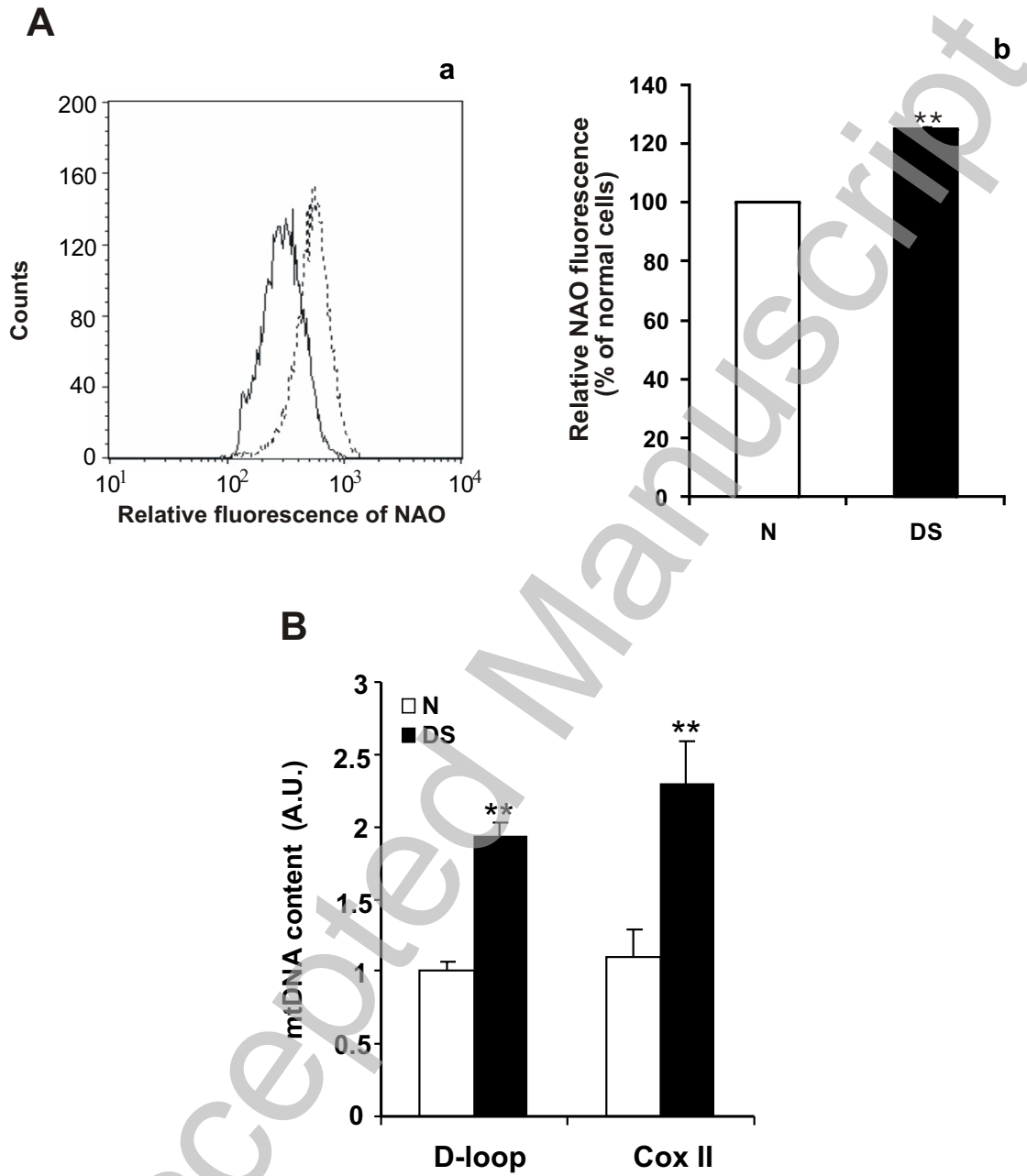
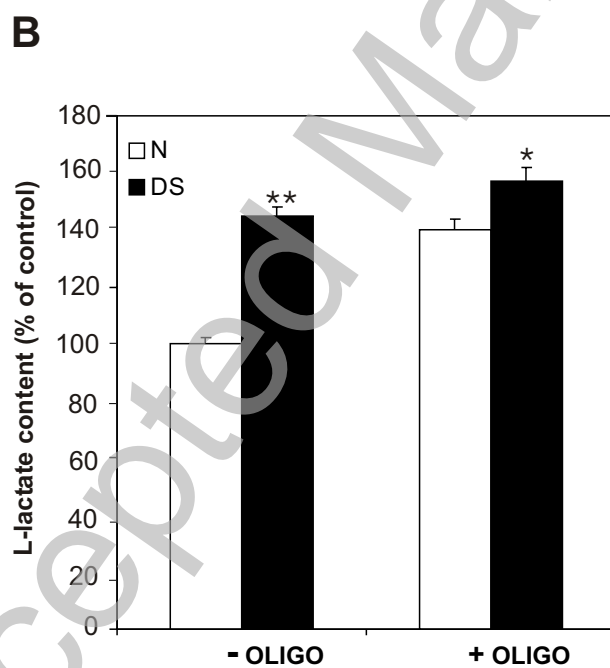
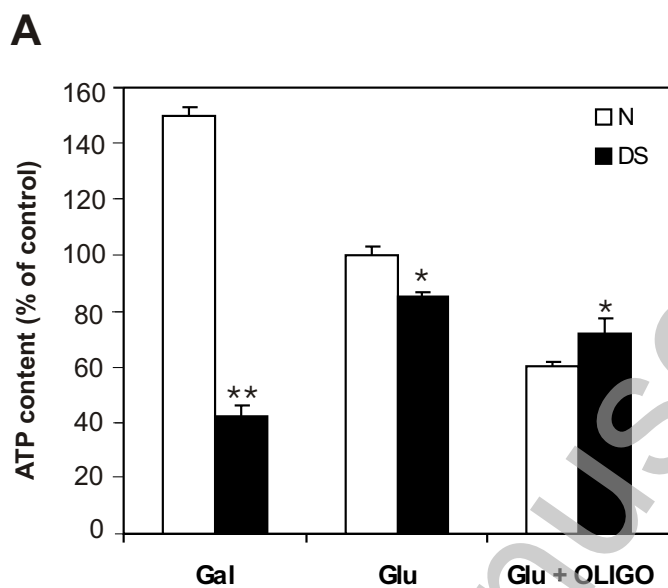


Fig. 6



THIS IS NOT THE VERSION OF THE ACCEPTED MANUSCRIPT. THIS IS NOT THE VERSION OF THE ACCEPTED MANUSCRIPT. THIS IS NOT THE VERSION OF THE ACCEPTED MANUSCRIPT.

Fig. 7



THIS IS NOT THE VERSION OF THE MANUSCRIPT. PLEASE REFER TO THE ACCEPTED MANUSCRIPT FOR THE FINAL VERSION.